

Analysis of the vibronic spectrum of chromium doped strontium titanate*

Quiesup Kim[†] and Richard C. Powell

Physics Department, Oklahoma State University, Stillwater, Oklahoma 74074

Mark Mostoller and Timothy M. Wilson[‡]

Solid State Division, Oak Ridge National Laboratory, Oak Ridge, Tennessee 37830

(Received 24 March 1975)

The fluorescence spectrum of chromium-doped strontium titanate was measured as a function of temperature. The low-energy vibronic sideband of the *R* lines at low temperatures was analyzed to determine the one-phonon and multiphonon contributions to the observed spectral profile. The one-phonon spectrum appears to be predominantly forced electric dipole in nature. Vibronic selection rules appropriate for such transitions were determined, and by comparison with neutron scattering and infrared absorption data more than 30 peaks in the vibronic spectrum can be tentatively identified with transitions involving specific phonon modes. Numerous low-frequency peaks are observed in the high-energy vibronic sideband, many of which cannot be associated with known vibrational modes. Using a simple long-wavelength phonon approximation, a phonon density of states is obtained and found to compare quite well to that determined from analyzing neutron scattering data. The temperature dependences of the widths of the zero-phonon lines and local mode were investigated using several phonon distributions including the effective density of phonon states obtained from the vibronic sideband. Low-frequency modes appear to make the dominant contribution to the broadening of the zero-phonon lines, whereas both low- and high-frequency phonons are active in broadening the local mode.

I. INTRODUCTION

Strontium titanate is a popular host for investigations of vibronic spectra because of the importance of lattice vibrations in determining the interesting structural, electrical, and acoustical properties of the material. It has the cubic perovskite structure at room temperature with one molecule per unit cell and O_h space-group symmetry. Around 110 K a second- or higher-order phase transition takes place and the symmetry becomes tetragonal. X-ray analysis implies that there are perhaps two other phase transitions at 65 and 35 K which further lower the symmetry.¹ The lattice dynamics of strontium titanate have been studied experimentally and theoretically.²⁻⁴ The phase transition at 110 K has also been the subject of numerous and varied investigations and is currently attributed to the precipitation of the lowest transverse-optic "soft" phonon mode at the corner of the Brillouin zone.^{1,4-6} The 35-K phase transition is associated with the soft mode at the corner of the zone.^{4,5}

Previous studies of the optical properties of ions in SrTiO_3 have centered around Eu^{3+} and Cr^{3+} , and some work has been done on a few other rare-earth and transition-metal ions. From ionic-size considerations and electron-spin-resonance data it is generally presumed that the rare-earth ions substitute for Sr^{2+} ions and the transition-metal ions go into Ti^{4+} sites. Charge compensation has been found to take place nonlocally.⁷ Both the strontium and titanium ions have O_h site symmetry

in the high-temperature phase of the lattice. The vibronic spectrum of europium-doped strontium titanate has been reported by Weber and Schaufele⁸ and that of chromium-doped strontium titanate has been reported by Stokowski and Schawlow⁹ and by Grabner.¹⁰ Although the Eu^{3+} vibronics appear only as weak, unresolved structure on the side of the zero-phonon line, several peaks can be associated with specific phonon modes through the calculation of vibronic selection rules and comparison with other data. The Cr^{3+} vibronic sideband exhibits much more pronounced structure. Although no detailed analysis has been made in this case, comparison with other data has led to the association of several vibronic peaks with specific phonon modes.

In this paper we report the results of a detailed investigation of the vibronic spectra of chromium-doped strontium titanate. An analysis of the low-energy (phonon emission) fluorescence vibronic sideband at low temperatures implies that the nature of the electronic part of the vibronic transition is predominantly forced electric dipole. Based on this result, vibronic selection rules were determined for phonons at various points in the Brillouin zone. Then by comparison with neutron scattering and infrared-absorption data, and by taking into account the vibronic selection rules, the peaks in the one-phonon contribution to the vibronic spectra were associated with transitions involving specific phonon modes. The high-energy (phonon-absorption) fluorescence vibronic sideband was investigated to better observe the low-

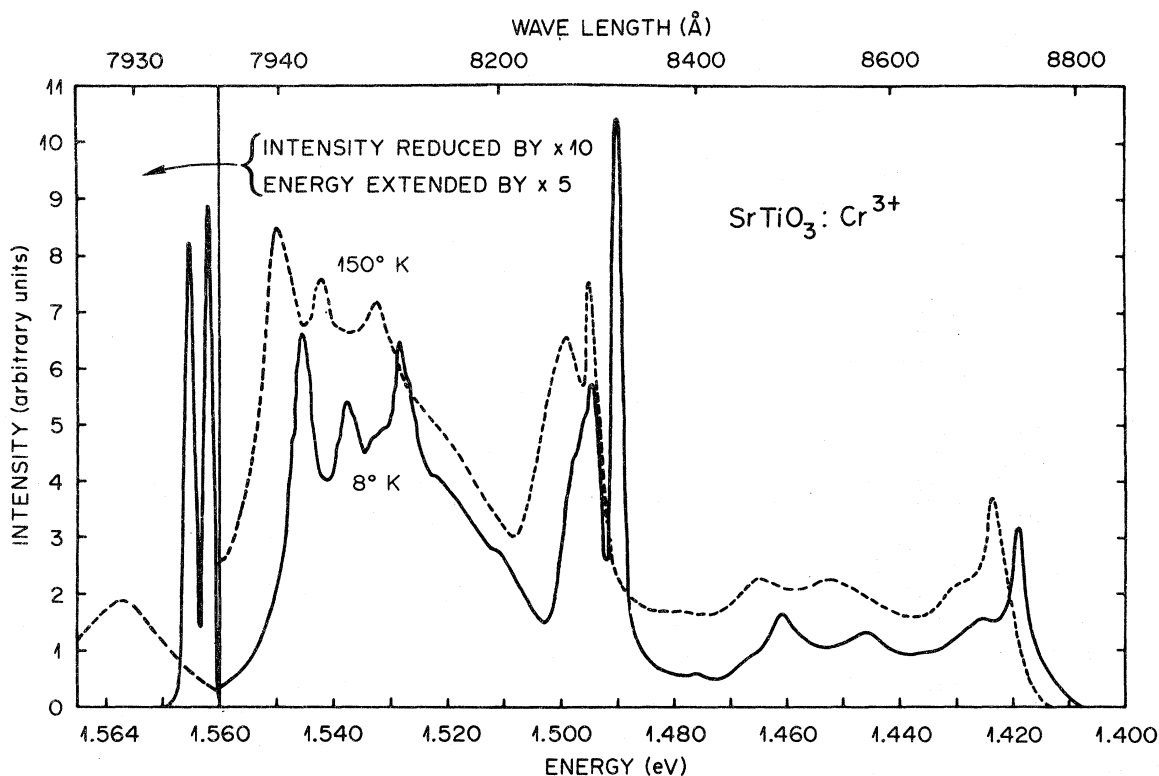


FIG. 1. Fluorescence spectrum of $\text{SrTiO}_3:\text{Cr}^{3+}$ at about 8 and 150 K.

frequency phonons, especially the soft transverse-optic modes. An effective density of phonon states was determined from the projected one-phonon vibronic sideband. This was used to obtain an estimate of the real phonon density of states and compared to that determined from fitting lattice-dynamics calculations to neutron scattering data. The effective density of states obtained from the vibronic spectra was also used in fitting the temperature dependence of the widths and positions of the zero-phonon lines and the widths, positions, and intensities of an impurity-induced local mode.

The experimental procedure is described briefly in Sec. II, and the analysis of the vibronic sidebands is presented in Sec. III. The temperature dependence of the widths of the zero-phonon lines and the local mode is discussed in Sec. IV.

II. EXPERIMENTAL

The $\text{SrTiO}_3:\text{Cr}^{3+}$ crystal used in these experiments was obtained from the National Lead Co. and contained 0.02% Cr_2O_3 by weight. It was mounted on the cold finger of an Air Products Displex Helium refrigerator capable of varying the temperature from about 8 K to room temperature.

For measuring the fluorescence spectrum, the

sample was illuminated with light from an AH-6 1000-W high-pressure mercury lamp filtered through 4 cm of saturated CuSO_4 . The fluorescence emission was chopped and focused onto the entrance slit of a Spex 1-m scanning monochromator. The signal was detected by a cooled RCA C31034 photomultiplier tube, amplified by a PAR model 128 lock-in amplifier, and recorded on a strip-chart recorder.

Fluorescence decay times were made using a Xenon Corporation Model 457 Nanopulser with a pulse width of 10 nsec as an excitation source. The signal was built up using single photon counting and multichannel scaling techniques with a 256 channel multichannel analyzer.

Figure 1 shows the fluorescence spectrum of $\text{SrTiO}_3:\text{Cr}^{3+}$ at about 8 and 150 K. At low temperatures the sharp zero-phonon lines (R_1 and R_2) are split by about 4.4×10^{-4} eV whereas in the high-temperature cubic phase only one R line appears. The low-energy vibronic sideband appears as a series of peaks spread over a range of about 0.15 eV from the R lines. The intense, sharp peak at 1.491 eV in the low-temperature spectrum has been attributed by Stokowski and Schawlow⁹ to an impurity-induced local mode because it does not correspond to any known phonon frequency of

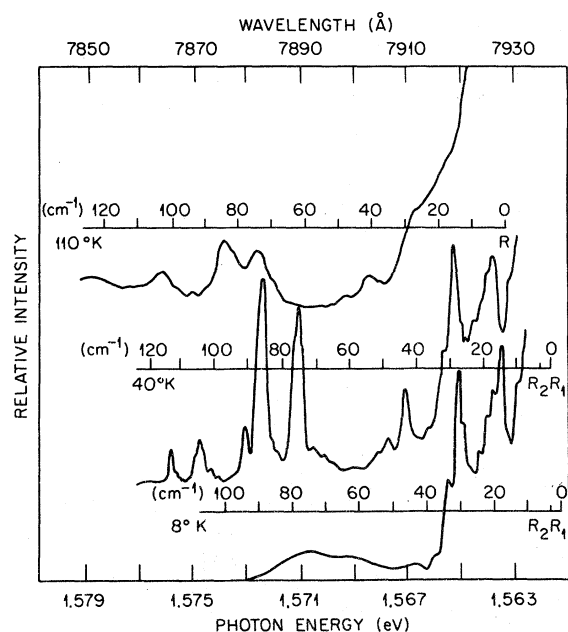


FIG. 2. High-energy fluorescence vibronic sideband of $\text{SrTiO}_3:\text{Cr}^{3+}$ at three temperatures.

strontium titanate and it does not appear in the vibronic sideband of Mn^{4+} in SrTiO_3 . Since the normal-mode phonon frequencies in SrTiO_3 extend to about 0.1 eV from the R lines, the observed sharp peak in the spectrum is not a local mode in the strict definition. It lies on the high-energy side of a host phonon peak containing contributions from $\text{TO}_4(\Gamma)$ and $\text{LO}_3(\Lambda)$ modes among others.²⁻⁴ As shown in Fig. 1, it is more like a gap mode at low temperatures and a band resonant mode at high temperatures. However, for simplicity's sake we will continue to refer to it as a local mode. The first harmonic of the local mode appears at about twice the separation from the R lines as the fundamental. As the temperature increases, the R lines broaden, shift to higher energy, and decrease in intensity, and their splitting decreases. Similarly, the local mode broadens, decreases in intensity, and shifts to lower energy relative to the R lines. The rest of the vibronic sideband increases in intensity as the temperature increases, and the structure becomes less distinct.

Among the more interesting phonon modes in strontium titanate are the low-frequency transverse-optic modes, which lie within about 0.015 eV of the zero-phonon lines in the vibronic spectrum. Although some faint structure is observed in this region in the low-energy, phonon emission sideband of Cr^{3+} shown in Fig. 1, it appears on the side of the broad, intense peak 0.015 eV below the R lines whose tail extends throughout this region. In an attempt to observe these low-frequency

modes more distinctly, we also measured the vibronic sideband on the high-energy, or phonon absorption side of the R lines. At low temperatures, the high-energy vibronic transitions are less intense than the corresponding low-energy transitions due to the lack of phonons available for absorption, but the low-frequency phonon modes of interest here are populated at rather modest temperatures. Figure 2 shows the high-energy vibronic spectrum at three different temperatures. More than 20 peaks can be observed in these spectra within 0.015 eV of the zero-phonon lines, which represents more low-frequency structure in the phonon spectrum than has been seen by any other technique.

It is interesting to observe that the intensities of most of the prominent peaks in the phonon absorption sideband do not increase with temperature proportionally to the phonon occupation numbers as expected. Instead, the intensities increase to a maximum at about 40 K and then decrease. A similar temperature dependence has been observed for the intensities of some of the low-frequency neutron scattering peaks.⁴ For soft modes this can be explained by the temperature dependence of the phonon frequency, which appears in the denominator of the expression for the transition rate. It would be interesting to observe the frequency shifts of the soft modes near the 110-K phase transition. Unfortunately, by this temperature the R lines have broadened and the vibronics have decreased in intensity to such an extent that it is difficult to observe this effect.

Table I lists the vibronic peaks observed in both the high-energy and low-energy, or phonon absorption and emission, sidebands at low temperatures.

Figure 3 shows the fluorescence decay time as a function of temperature. It is about 17.8 msec at 10 K and decreases above about 100 K. The solid line represents the ratio of the integrated intensity of the R lines to that of the total spectrum, adjusted to fit the decay time data. If radiationless processes are not important, this intensity ratio is related to the fluorescence lifetime τ_F by

$$I_R/I_T = W_R \tau_F, \quad (1)$$

and the radiative transition rate W_R is generally independent of temperature. Figure 3 shows that the intensity ratio is proportional to the decay time at low temperatures, but the fact that the solid line falls below the lifetime data above 100 K indicates the increasing importance of radiationless decay processes in this temperature range.

III. VIBRONIC SIDEBANDS

The fluorescence spectrum of $\text{SrTiO}_3:\text{Cr}^{3+}$ appears to be an interesting mixture of magnetic

TABLE I. Vibrational modes of SrTiO₃ appearing in vibronic, infrared absorption, Raman scattering, and neutron scattering spectra (in units of 10⁻² eV).

Vibronics (°K)		Pure SrTiO ₃ (°K)			Assignment mode (point)
Cr ³⁺	Mn ⁴⁺ or Eu ³⁺	Infrared	Raman	Neutron	
H ^a 0.15(40)					
H 0.21(40)			0.19(40) ^b	0.19(60) ^c 0.19(40) ^d	TO ₁ (R)
H 0.22(40)					
H 0.27(40)					
H 0.31(40)					
H 0.34(40)					
H 0.36(40)			0.27(40) ^b 0.35(40) ^e 0.35(8) ^b	0.27(40) ^d 0.5(90) ^c	TO ₁ (Γ)
H 0.38(40)			0.37(79) ^f		Local mode
H 0.46(40)					
H 0.51(40)					
			0.41(78) ^g 0.55(77) ^e 0.55(40) ^b 0.56(20) ^f 0.61(4) ^h 0.62(125) ⁱ	0.40(60) ^c 0.53(40) ^e	TO ₁ (R)
H 0.55(40)	H 0.57(100)				
H 0.60(40)					
H 0.65(40)	H 0.68(100) ^j				
H 0.71(40)					
H 0.81(40)			0.82(125) ⁱ	0.81(120) ^d 0.87(78) ^c	TA ₁ (M)
H 0.84(40)					
H 0.88(40)					
H 0.93(40)			0.91(78) ^g 0.93(78) ^h 0.97(77) ^e 1.01(79) ^f		
H 1.07(40)					
H 1.13(40)					
H 1.25(40)					
H 1.29(40)				1.30(120) ^d 1.34(297) ^c	TA ₁ (Σ)
1.30(4) ^k					
1.368(8.4)	1.327(20.4) ^l			1.33(90) ^c	LA ₁ (Λ)
1.346(20.4) ^l				1.38(297) ^f 1.43(297) ^c	TO ₁ (M), TA ₁ (M) LA ₁ (X)
H 1.40(40)			1.45(125) ^j	1.45(297) ^c (120) ^d	TO ₁ (M)
H 1.51(40)				1.49(297) ^c (120) ^d	LA ₁ (M) TA ₁ (Λ), LA ₁ (Λ)
1.50(4) ^k				1.470(297) ^c	TA ₁ (X)
1.315(20.4) ^l					
1.483(8.4)	1.486(20.4) ^l			1.491(297) ^c	LA ₁ (M)
1.485(20.4) ^l					
1.637(8.4)	1.564(20.4) ^l				
1.533(20.4) ^l					
1.65(4) ^l	1.639(20.4) ^l			1.651(296) ^c	TO ₁ (Δ)
1.50(4) ^k					
1.869(8.4)				1.805(297) ^c	LO ₁ (R), TO ₁ (R)
1.688(20.4) ^l	1.787(20.4) ^l			1.862(296) ^c	LA ₁ (X)

TABLE I. (Continued)

Vibronics (°K)		Pure SrTiO ₃ (°K)			Assignment mode (point)
Cr ³⁺	Mn ⁴⁺ or Eu ³⁺	Infrared	Raman	Neutron	
2.11(4) ^h	2.234(20.4) ¹	2.115(300) ^m		2.073(296) ^c	LO ₁ (Γ)
2.310(8.4)		2.210(300) ^o		2.110(297) ^c	
2.197(20.4) ¹		2.296(300) ^p			
2.20(4) ^k		2.185(300) ^q			TO ₂ (Γ)
2.48(4) ^k	2.334(20.4) ¹				
2.405(8.4)					
2.321(20.4) ¹					
2.558(8.4)				2.321(296) ^c	TO ₂ (X)
2.38(4) ^k				2.434(297) ^c	
2.730(8.4)					
2.881(8.4)	2.855(20.4) ¹			2.855(296) ^c	2TA ₁ (X), 2TO ₁ (X)
2.867(20.4) ¹					
3.10(4) ^k	3.041(20.4) ¹				
3.071(8.4)			3.103(300) ^h		TO ₃ (Γ)
3.078(20.4) ¹					
3.222(8.4)	3.265(20.4) ¹				
3.252(20.4) ¹					
3.10(4) ^k			3.116(300) ^f	3.289(297) ^c	LO ₂ (Γ), TO ₃ (Γ)
3.30(4) ^k	3.426(20.4) ¹			3.395(297) ^f	LO ₁ (X)
3.393(8.4)					
3.426(20.4) ¹					
3.50(4) ^k				3.478(297) ^c	LO ₁ (M)
			3.823(300) ^f	3.602(297) ^c	LO ₂ (X)
			3.848(300) ^h		
3.95(4) ^k				4.079(297) ^c	TO ₃ (X)
3.899(8.4)				4.120(297) ^c	TO ₃ (M)
3.923(20.4) ¹				5.549(297) ^c	TO ₃ (R)
			4.580(300) ^f		
			4.469(300) ^h	5.590(297) ^c	TO ₂ (R), LO ₂ (R)
			4.717(300) ^h		
5.70(4) ^k	4.791(20.4) ¹	5.871(300) ^o		4.673(297) ^c	LO ₃ (Γ)
	4.710(77) ⁿ				
			5.524(4) ^h		
6.40(4) ^k				5.809(297) ^c	LO ₂ (M)
6.260(8.4)				5.880(297) ^c	LO ₃ (R)
6.219(20.4) ¹					
6.459(8.4)	6.356(20.4) ¹				LO ₂ (X)
6.430(20.4) ^k					
6.78(4) ^k	6.827(77) ⁿ	6.778(300) ^o		6.790(297) ^c	TO ₄ (Γ)
6.622(8.4)		6.889(300) ^p			
6.616(20.4) ¹					
			7.696(300) ^h		
			7.808(300) ^f		
7.054(8.4)					Local mode TO ₄ (X)
7.044(20.4) ¹					
7.20(4) ^k					
8.391(20.4) ¹	8.342(20.4) ¹		8.379(300) ^h	8.143(296) ^c	2TO ₃ (X)
			8.491(300) ^f		
9.319(8.4)			8.937(300) ^h		
9.260(20.4) ¹			9.024(300) ^f		

TABLE I. (Continued)

Vibronics ($^{\circ}\text{K}$)		Pure SrTiO_3 ($^{\circ}\text{K}$)			Assignment mode (point)
Cr^{3+}	Mn^{4+} or Eu^{3+}	Infrared	Raman	Neutron	
11.60(4) ^k			9,186(300) ^h		$\text{LO}_4(X)$
10.0(4) ^k					
9.926(8,4)	10.377(20.4) ^l	9.980(300) ^m		10.227(297) ^f	$\text{LO}_4(\Gamma)$
9.881(20.4) ^l	9.806(77) ^u				
10.664(8,4)					
11.430(8,4) ^l					
11.445(20.4) ^l	10.799(20.4) ^l				
13.252(8,4)			12,786(300) ^h		
13.195(20.4)	12.438(20.4) ^l		12,885(300) ^f		
14.203(8,4)					
15.417(20.4) ^l	14.114(20.4) ^l		16,447(300) ^f		2 (Local mode)

^kH: high-energy sideband.

^lReference 5.

^mReferences 2 and 3.

^uReference 4.

^hD. C. O'Shea, R. V. Kolluri, and H. Z. Cummins, *Solid State Commun.* **5**, 241 (1967).

^lW. F. Nilsen and J. G. Skinner, *J. Chem. Phys.* **48**, 2240 (1968).

^mR. F. Schaufele and M. J. Weber, *J. Chem. Phys.* **46**, 1859 (1967).

^fC. H. Perry, J. H. Fertel, and T. F. McNelly, *J. Chem. Phys.* **47**, 1619 (1967).

^hL. Rimai and J. L. Parsons, *Solid State Commun.* **5**, 387 (1967).

^fH. Yamamoto, S. Makishima, and S. Shionoya, *J. Phys. Soc. Jpn.* **23**, 1321 (1967).

^lReference 10.

^mReference 9.

^hReference 20.

^fReference 8.

^lReference 19.

^mReference 21.

^fReference 22.

dipole and phonon-forced electric dipole transitions. Burke and Pressley¹¹ have investigated the Zeeman spectra of $\text{SrTiO}_3:\text{Cr}^{3+}$ and concluded that the R_1 and R_2 zero-phonon lines arise from magnetic dipole transitions between the 2E_g excited state and the ${}^4A_{1g}$ ground state, which are split by small amounts at low temperatures by the noncubic distortions of the lattice. The same conclusion was reached by Stokowski and Schawlow⁹ on the basis of studies of the polarization dependence of the intensity ratio of the R_1 and R_2 lines.

The vibronic sidebands, at least in the one-phonon energy range, appear to be largely electric dipole in origin. While electric dipole transitions between electronic states of the same parity are normally forbidden, they can become allowed if the electron-phonon interaction mixes in electronic states of opposite parity. For the 8-K fluorescence spectrum shown in Fig. 1, the ratio of the integrated intensity of the zero-phonon lines to that of the vibronic sideband is roughly 0.39. If the sideband were all magnetic dipole in nature, this would correspond to a total Huang-Rhys factor of about 0.95. With a Huang-Rhys factor of this magnitude, two phonon emission processes would make substantial contributions to the total spectrum, and as we will see in more detail later, the near gap just above the local mode would not occur. As

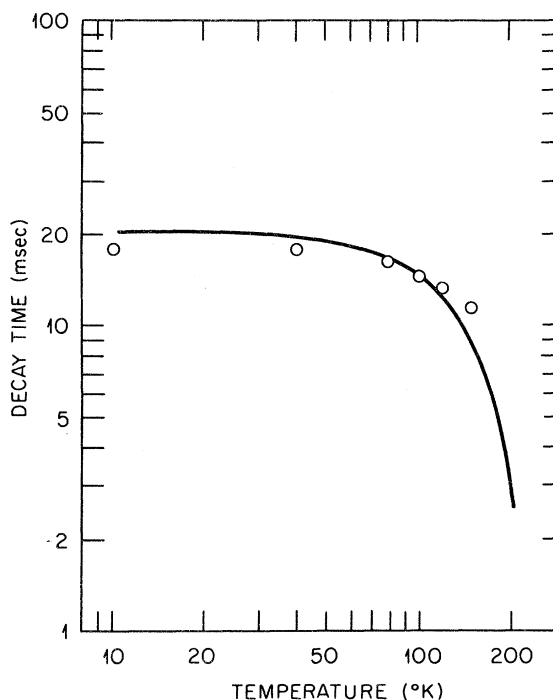


FIG. 3. Temperature dependence of the fluorescence lifetime of Cr^{3+} in SrTiO_3 . Circles represent experimental data. The solid line is the integrated intensity ratio given in Eq. (1) with $W_R = 18.3 \text{ sec}^{-1}$.

previously mentioned, the phonon density of states in pure SrTiO_3 extends up to an energy of approximately 0.1 eV.³ The fluorescence spectrum of $\text{SrTiO}_3:\text{Cr}^{3+}$ appears to be dominated by one-phonon processes, and extends only into the two-phonon range. This is consistent with vibronic sidebands produced by phonon-forced electric dipole transitions. However, magnetic dipole transitions may also contribute to the sidebands, particularly if their intensity is concentrated in narrow frequency regions.

The frequency dependence of the spectral intensity near the zero-phonon lines provides further evidence that the sidebands are primarily forced electric dipole in nature. Vredevoe¹² has studied the shape of the one-phonon spectrum in the limit of long phonon wavelengths for substitutional impurity ions in the rock-salt and zinc-blende structures. In the zinc-blende lattice, he found that the sideband intensity should be proportional to $|\omega - \omega_0|^3$ for forced electric dipole transitions, and to $|\omega - \omega_0|$ for magnetic dipole transitions, where $\omega - \omega_0$ is the photon frequency relative to the zero-phonon line. In the rock-salt lattice, the intensity near the zero-phonon line varies as $|\omega - \omega_0|^5$ and $|\omega - \omega_0|^3$ for forced electric dipole and magnetic dipole transitions, respectively.

The low-temperature phases of SrTiO_3 , like the zinc-blende lattice, do not have inversion symmetry. As indicated by the small splitting of the R lines at 8 K and the insensitivity of the sideband structure to the phase transition at 110 K, the low-temperature distortions away from O_h symmetry have an essentially negligible effect on the vibronic spectrum over most of its frequency range. However, the very low (relative) frequency behavior of the sideband will be determined by the noncubic distortions if magnetic dipole transitions are dominant at these frequencies, since this would give an $|\omega - \omega_0|$ dependence rather than some higher power law.

Figure 4 shows the intensity of the phonon emission sideband as a function of relative photon energy at 8 K in the region very close to the R lines. Our data are found to vary as

$$I = a + b_1(\omega_{10} - \omega)^3 + b_2(\omega_{20} - \omega)^3, \quad (2)$$

where ω_{10} and ω_{20} are the R_1 and R_2 line peak frequencies and the constants a , b_1 , and b_2 have the values 2.73, 0.086, and 0.081, respectively. The additive constant in Eq. (2) may be due to the effects of microscopic strain. The good fit to the long-wavelength tail of the low-temperature spectrum which is obtained with a third-power-law dependence on the relative photon frequency is consistent with forced electric dipole transitions.

Vibronic sidebands arise, of course, from phonon-impurity electron interactions. The kinds of

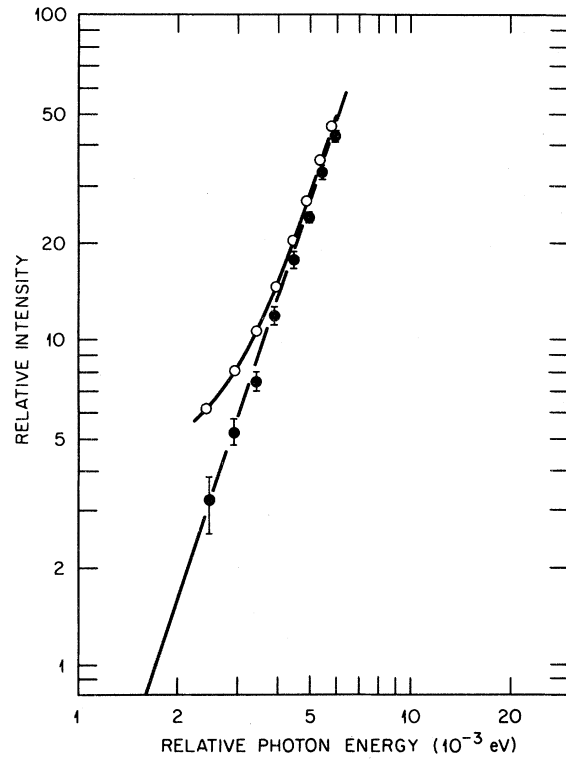


FIG. 4. Intensity of the low-energy fluorescence vibronic sideband close to the zero-phonon lines at 8 K. The curve is the measured intensity and the straight line is obtained after subtracting a constant to fit Eq. (2). The best fit is obtained with $a = 2.73$, $b_1 = 0.086$, and $b_2 = 0.081$.

interaction terms of interest for the $\text{SrTiO}_3:\text{Cr}^{3+}$ spectrum are well illustrated by the point-charge model, which is the model used by Vredevoe. The impurity lattice site is taken as the origin, and \vec{r} is the electronic coordinate relative to the impurity ion core. $\vec{R}(l)$, $\vec{u}(l)$, and $z(l)$ denote the equilibrium position, displacement from equilibrium, and effective charge, respectively, of the ion at the site l . With the assumptions that $|\vec{r}| \ll |\vec{R}(l)|$ and $|\vec{u}(l) - \vec{u}(0)| \ll |\vec{R}(l)|$, the crystal potential energy of the impurity electron can be expanded in a Taylor series,

$$\begin{aligned} v(\vec{r}) = & - \sum_l' \frac{e^2 z(l)}{|\vec{R}(l) - \vec{r}|} + \sum_l' \frac{e^2 z(l)}{|\vec{R}(l)|^3} \{ \vec{R}(l) \cdot [\vec{u}(l) - \vec{u}(0)] \\ & + \frac{1}{2} [\vec{u}(l) - \vec{u}(0)] \cdot \underline{D}(\vec{R}(l)) \cdot [\vec{u}(l) - \vec{u}(0)] \} \\ & - \sum_l' \frac{e^2 z(l)}{|\vec{R}(l)|^3} \vec{r} \cdot \underline{D}(\vec{R}(l)) \cdot [\vec{u}(l) - \vec{u}(0)] + \dots \end{aligned} \quad (3)$$

Here \sum_l' denotes the sum over sites $l \neq 0$, and $\underline{D}(\vec{x})$ is the dipole-dipole tensor,

$$D_{\alpha\beta}(\vec{x}) = \delta_{\alpha\beta} - 3x_\alpha x_\beta / |\vec{x}|^2.$$

The first term in Eq. (3) does not involve the ionic displacements; it affects only the static electronic energy levels, and cannot give rise to any vibronic structure in any optical transition. The second two terms are linear and quadratic in the ionic displacements, but do not involve the electronic coordinate. The matrix elements of these terms are therefore diagonal in the electronic states, and can by themselves produce vibronic sidebands only for allowed transitions, that is, for electric dipole transitions between electronic states of opposite parity or magnetic dipole transitions between electronic states of the same parity. The final term is bilinear in the electronic and phonon coordinates. For any electronic state, this term gives a dynamic admixture of states of opposite parity. Such an interaction allows electric dipole transitions between electronic states of the same parity, or magnetic dipole transitions between states of opposite parity. In the two-phonon and higher-order contributions to the total spectrum, interaction terms like the second and last in Eq. (3) can act in combination to yield structure which neither term could produce independently.

The full Hamiltonian for the impurity electron-phonon system can be written in the form

$$H = H_e + H_p + H_{ep}, \quad (4)$$

$$H_e = \sum_m |\psi_m\rangle \epsilon_m \langle \psi_m|, \quad (5)$$

$$H_p = \sum_\lambda \hbar \omega_\lambda (a_\lambda^\dagger a_\lambda + \frac{1}{2}), \quad (6)$$

$$H_{ep} = \sum_{mm'} |\psi_m\rangle I_{mm'}(\{a_\lambda, a_\lambda^\dagger\}) \langle \psi_{m'}|. \quad (7)$$

Here $|\psi_m\rangle$ is an unperturbed electronic state, and a_λ (a_λ^\dagger) is the destruction (creation) operator for the phonon mode λ of frequency ω_λ . In general, it is most convenient to diagonalize the phonon Hamiltonian in the initial electronic state of the optical transition of interest, in which case λ denotes the phonon modes for the impurity in its initial state.¹³⁻¹⁶ In the electron-phonon interaction Hamiltonian H_{ep} , $I_{mm'}(\{a_\lambda, a_\lambda^\dagger\})$ is a phonon operator which may include not only linear but higher-order terms in a_λ and a_λ^\dagger . The second and third terms in Eq. (3), for example, make contributions to $I_{mm'}$ which are diagonal in the electronic states ($m = m'$) and first and second order, respectively, in the phonon creation and destruction operators. The last term in Eq. (3) mixes electronic states of opposite parity and is linear in a_λ and a_λ^\dagger .

The symmetry of the phonon operators $I_{mm'}$ can be determined from the transformation properties of the electronic states $|\psi_m\rangle$, $|\psi_{m'}\rangle$ and the point

group of the defect. As previously noted, the non-cubic distortions of the SrTiO₃ lattice in its low-temperature phases appear to have very minor effects on the sidebands, so we will assume O_h site symmetry for our discussion of phonon selection rules. The Hamiltonian must be invariant under the operations of the point group, that is, it must transform as the totally symmetric (A_{1g}) representation of O_h . If the electronic states $|\psi_m\rangle$ and $|\psi_{m'}\rangle$ transform according to the representations $\Gamma(m)$ and $\Gamma(m')$, then the allowed symmetries of the phonon operator $I_{mm'}(\{a_\lambda, a_\lambda^\dagger\})$ are those representations contained in the direct product $\Gamma(m) \times \Gamma(m')$. Through quadratic coupling terms, we have

$$I_{mm'} = \sum_{\gamma p} \left(\sum_\lambda V_{mm'}(\lambda; \gamma p)(a_\lambda + a_\lambda^\dagger) + \frac{1}{2} \sum_{\lambda, \lambda'} W_{mm'}(\lambda, \lambda'; \gamma p)(a_\lambda + a_\lambda^\dagger)(a_{\lambda'} + a_{\lambda'}^\dagger) \right), \quad (8)$$

where γ runs over the irreducible representation (IR's) contained in $\Gamma(m) \times \Gamma(m')$ and p labels the members of the various IR basis sets. For simplicity, we have assumed that no IR γ occurs more than once in $\Gamma(m) \times \Gamma(m')$, and that the phonon creation and destruction operators appear in the combination $a_\lambda + a_\lambda^\dagger$, but these simplifying assumptions can readily be lifted.

For allowed electric or magnetic dipole transitions, diagonal interactions $|\psi_m\rangle I_{mm} \langle \psi_m|$ in the final and initial states are generally responsible for the sidebands.¹⁶⁻¹⁹ For the SrTiO₃:Cr³⁺ fluorescence spectrum, the initial- and final-state direct products are $E_g \times E_g = A_{1g} + A_{2g} + E_g$ and $A_{2g} \times A_{2g} = A_{1g}$. Thus only A_{1g} , A_{2g} , and E_g phonons or combinations of phonons may appear in any magnetic dipole contributions to the sidebands. The linear coupling terms in Eq. (8) for $m = m' = A_{2g}$, E_g can involve only A_{1g} , A_{2g} , or E_g phonons. In the quadratic coupling terms, however, while the product operators must transform as one of these even modes, the factors in the products may be both even or both odd. For example, $T_{1u} \times T_{1u} = A_{1g} + E_g + T_{2g} + T_{1g}$, so pairs of T_{1u} phonons give a quadratic coupling term of acceptable (A_{1g} or E_g) symmetry.

The matrix elements for the phonon-forced electric dipole sidebands of the SrTiO₃:Cr³⁺ R lines involve products of the form $\langle \psi_f | \vec{r} | \psi_m \rangle I_{mi}$ and $I_{fm} \langle \psi_m | \vec{r} | \psi_i \rangle$, where $f = A_{2g}$ and $i = E_g \theta, \epsilon$, and $|\psi_m\rangle$ is an odd intermediate state. The electric dipole operator \vec{r} transforms as T_{1u} , so the allowed intermediate states must transform as T_{1u} or T_{2u} since $A_{2g} \times T_{1u} = T_{2u}$ and $E_g \times T_{1u} = T_{1u} + T_{2u}$. The phonon coupling operators I_{mi} and I_{fm} must then transform according to T_{1u} or T_{2u} . An equivalent but more direct demonstration of the same conclusion is

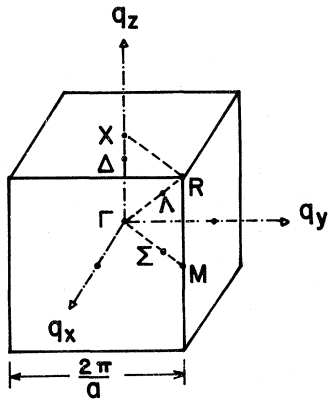


FIG. 5. First Brillouin zone of SrTiO_3 with points of high symmetry labeled.

provided by the triple direct product $E_g \times T_{1u} \times A_{2g} = T_{1u} + T_{2u}$.

The Brillouin zone (BZ) for SrTiO_3 is shown in Fig. 5 with points of high symmetry indicated. There are fifteen phonon modes at each point in the Brillouin zone. The transformation properties of the phonons along the principal symmetry directions have been determined by Cowley.² We wish, however, to know the projections of the phonon modes at the various points in the BZ onto the IR's of the point group of the defect, O_h . If the O_h projection of a phonon mode contains T_{1u} or T_{2u} , then the phonon can contribute to the forced electric dipole sideband. If it does not contain one of these two modes, then electric dipole transitions involving such phonons are forbidden. Table II summarizes the vibronic selection rules obtained for transitions from an E_g state to other even electronic states. The majority of the phonon modes are allowed for $E_g \rightarrow A_{2g}$ transitions, but at the R , X , and M points, where the group of the wave vector has inversion symmetry, all of the even modes and some of the odd modes are forbidden.

Some of the peaks in the vibronic spectrum can now be tentatively identified with transitions involving specific phonon modes by comparing with other data and accounting for vibronic selection rules. Figure 6 shows the low-energy vibronic sideband at 8 K in comparison with neutron scattering curves for five different directions in the Brillouin zone. The circles at the Γ point represent frequencies observed in infrared absorption. The circle with the cross in it at 0.1023 eV indicates a mode observed in both infrared absorption and neutron scattering.

Vibronic peaks should occur wherever there is an allowed transition coupled with a high effective phonon density of states. In the perfect crystal,

the latter occurs where the dispersion curves have a slope of zero. These regions are designated by dashed lines in the center of the figure and can be seen to correspond with many of the vibronic peaks. Stirling³ has fitted the observed phonon dispersion curves with a shell model subjected to several sets of constraints. Table III summarizes the results he obtained at Γ , X , M , and R with the model (his model 5) which gave the best over-all agreement with experiment; the modes which are forbidden by the vibronic selection rules given in Table II are marked by a superscript b in Table III. Note that the predicted X -, M -, and R -point peaks between 0.04 and 0.06 eV are not allowed by the selection rules for forced electric dipole transitions, and that the observed vibronic structure in this region is weak.

TABLE II. Vibrational modes allowed in electric dipole transitions from an E_g state to other even electronic states. (x indicates allowed modes).

Point	Point group	IR	Final electronic states				
			A_{1g}	A_{2g}	E_g	T_{1g}	T_{2g}
Γ	O_h	T_{1u}	x	x	x	x	x
		T_{2u}	x	x	x	x	x
R	O_h	T_{2g}					
		A_{2u}				x	x
		E_u				x	x
		T_{1u}	x	x	x	x	x
		T_{2u}	x	x	x	x	x
M	D_{4h}	A_{1g}					
		A_{2g}					
		B_{1g}					
		B_{2g}					
		E_g					
		A_{2u}	x	x	x	x	x
		B_{1u}				x	x
X	D_{4h}	E_u	x	x	x	x	x
		A_{1g}					
		B_{1g}					
Δ	C_{4v}	E_g					
		A_{2u}	x	x	x	x	x
		E_u	x	x	x	x	x
		A_1	x	x	x	x	x
		B_1	x	x	x	x	x
Λ	C_{3v}	E	x	x	x	x	x
		A_1	x	x	x	x	x
		A_2	x	x	x	x	x
Σ	C_{2v}	E	x	x	x	x	x
		A_1	x	x	x	x	x
		A_2	x	x	x	x	x
		B_1	x	x	x	x	x
K	C_1	B_2	x	x	x	x	x
		A	x	x	x	x	x
		A	x	x	x	x	x

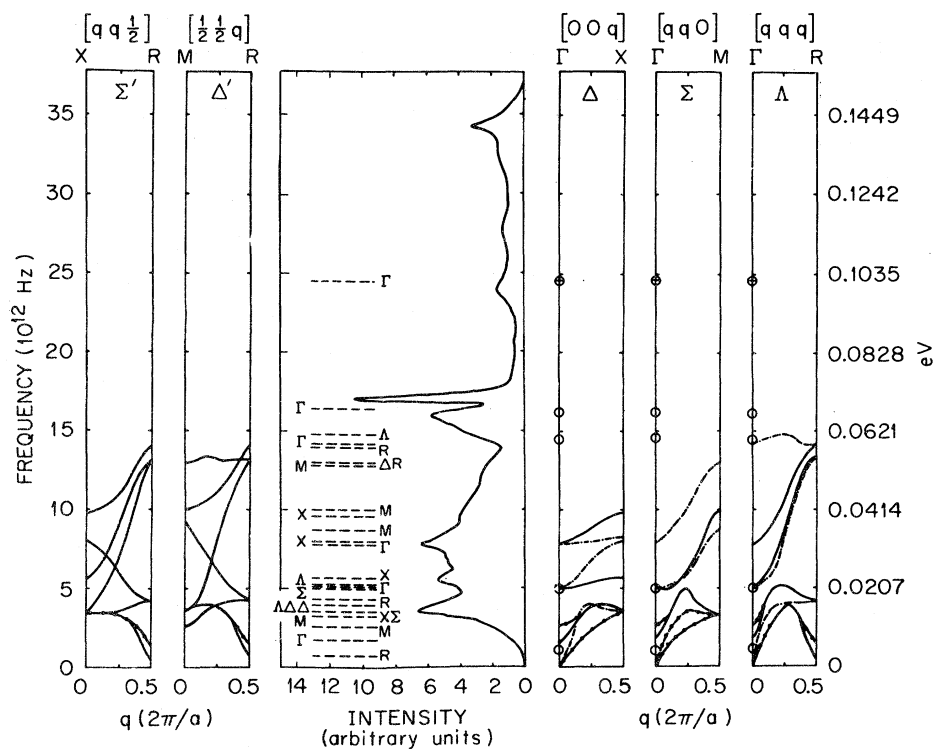


FIG. 6. Low-energy fluorescence vibronic sideband at 8 K in comparison with dispersion curves obtained from neutron scattering (Refs. 2 and 3). The solid and dashed lines represent transverse and longitudinal modes, respectively. The circles at Γ represent infrared data (Refs. 20–23) and the highest mode marked by \odot is seen in both neutron scattering and infrared absorption.

Table I shows the correlation between neutron scattering, infrared absorption, Raman scattering, and vibronic spectra data. First-order Raman scattering is allowed only in the low-temperature phase where the R point becomes the center of the Brillouin zone. Much of the detailed structure observed in the high-energy (phonon absorption) sideband can not be identified with specific phonon modes. Some of this may be associated with the vibronics of the R_2 line. Other peaks may be attributed to the splitting of some of the phonon modes due to the tetragonal distortion which is difficult to resolve in the less structured low-energy sideband. The phonon splittings in going from cubic to tetragonal (D_{4h}^{18}) symmetry have been worked out only at the R point.^{5,6} Some of these split components are identified in Table I. A total of about 36 vibronic peaks can be associated with specific phonon modes.

While it is relatively easy to account for the sidebands in the one-phonon region, it is more difficult to determine the origin of the observed spectrum from the local mode out through its first harmonic. For the sake of brevity, we will refer to this portion of the spectrum as the local-mode sideband. In the perfect-crystal density of states, there is one isolated peak above the local mode at $\hbar\omega \sim 0.1$ eV, which may give a one-phonon peak in the energy range of the local-mode sideband.

There may also be true local-mode peaks in this energy range, but their number must be limited to a few, if any, and their widths would necessarily be narrow since the concentration of Cr^{3+} impurities is very low. The bulk of the local-mode sideband must therefore arise from one or both of two sources: multiphonon processes within the linear coupling approximation, or quadratic or higher coupling. In addition, the local mode, its harmonic, and the local-mode sideband may have their origins, separately or together, in forced electric dipole or allowed magnetic dipole transitions. Symmetry arguments provide a check on the internal consistency of any proposed explanation of the total spectrum.

A reasonably good fit to the total spectrum could be obtained with a simple combination of linear and quadratic coupling if the sidebands, like the zero-phonon lines, were all allowed magnetic dipole in nature. Although this seems clearly not to be the case, the analysis is still instructive. Diagonal electron-phonon interactions I_{mm} in the final and initial states are assumed to be most important. In the quadratic coupling terms, only those products which include the local mode as one or both of their factors are retained. The simplest additional simplifying assumption that can then be made is that the quadratic coupling coefficients involving the local mode are proportional to

TABLE III. Vibrational mode energies at 297 K from neutron scattering data and predicted by the shell-model fit of Stirling.^a *T* and *L* label transverse and longitudinal modes, respectively, and energies are in units of 10⁻² eV.

Point	Modes (10 ⁻² eV)						
Γ	<i>T</i>	<i>T</i> _{1u}	<i>T</i> _{1u}	<i>T</i> _{1u}	<i>T</i> _{2u}		<i>T</i> _{1u}
	Expt.	0	1.14 ± 0.04	2.10 ± 0.04	3.29 ± 0.06		6.78 ± 0.04
	Theory	0	1.06	2.14	3.42		6.93
	<i>L</i>	<i>T</i> _{1u}		<i>T</i> _{1u}	<i>T</i> _{2u}	<i>T</i> _{1u}	<i>T</i> _{1u}
	Expt.	0		2.10 ± 0.04	3.29 ± 0.06	5.67 ± 0.21	10.21 ± 0.12
	Theory	0		2.11	3.42	6.10	0.06
X	<i>T</i>		<i>E</i> _g ^b	<i>E</i> _u	<i>E</i> _g ^b		<i>E</i> _u
	Expt.		1.47 ± 0.02	1.47 ± 0.02	2.43 ± 0.03		4.09 ± 0.08
	Theory		1.42	1.51	2.49		3.85
	<i>L</i>	<i>A</i> _{2u}			<i>A</i> _{1g} ^b	<i>B</i> _{1g} ^b	
	Expt.	1.43 ± 0.06			3.39 ± 0.03	3.60 ± 0.06	
	Theory	1.68			3.72	3.81	
M	<i>T</i>	<i>B</i> _{1g} ^b	<i>B</i> _{1u} ^b	<i>A</i> _{2u} ^b			<i>E</i> _g ^b
	Expt.	1.09 ± 0.02	1.38 ± 0.05	1.38 ± 0.05			4.11 ± 0.08
	Theory	0.83	1.34	1.50			3.78
	<i>L</i>				<i>E</i> _u	<i>E</i> _u	<i>A</i> _{1g} ^b
	Expt.				1.49 ± 0.06	3.47 ± 0.08	5.81 ± 0.10
	Theory				1.35	3.70	
R	<i>T</i>	<i>T</i> _{2u}	<i>T</i> _{1u}	<i>E</i> _u ^b	<i>T</i> _{1u}		
	Expt.	0.64 ± 0.02	1.80 ± 0.05	5.58 ± 0.08	5.54 ± 0.17		
	Theory	0.73	1.54	5.14	5.23		
	<i>L</i>	<i>T</i> _{2u}	<i>T</i> _{1u}	<i>T</i> _{1u}		<i>T</i> _{2g} ^b	
	Expt.	0.64 ± 0.02	1.80 ± 0.05	5.58 ± 0.08		5.87 ± 0.21	
	Theory	0.73	1.54	5.23		5.99	

^aReference 3.

^bForbidden by vibronic selection rules.

products of linear coupling coefficients,

$$W_{mm}(\lambda, \lambda') = \alpha V_{mm}(\lambda) V_{mm}(\lambda') (\delta_{\lambda L} + \delta_{\lambda' L} - \delta_{\lambda L} \delta_{\lambda' L}), \quad (9)$$

where *L* denotes the local mode, and the sum of Kronecker deltas in Eq. (9) is such that double counting is avoided for $\lambda = \lambda' = L$. From Eq. (8), the electron-phonon coupling operators *I*_{mm} then have the form

$$I_{mm} = \sum_{\lambda} V_{mm}(\lambda) (a_{\lambda} + a_{\lambda}^{\dagger}) + \frac{1}{2} \alpha \sum_{\lambda, \lambda'} V_{mm}(\lambda) \times V_{mm}(\lambda') (a_{\lambda} + a_{\lambda}^{\dagger}) (a_{\lambda'} + a_{\lambda'}^{\dagger}) (\delta_{\lambda L} + \delta_{\lambda' L} - \delta_{\lambda L} \delta_{\lambda' L}). \quad (10)$$

Equations (9) and (10) are written as if the local-mode peak had no width, but they are easily generalized to include the observed shape of the local-mode peak; this was done for the calculations discussed below.

With the interactions described by Eq. (10), the low-temperature fluorescence spectrum of SrTiO₃:Cr³⁺ can be fitted by the iterative deconvolution techniques applied by one of the authors

and co-workers to the optical spectra of the *N*₁ center in NaCl and the *M*(*C*_{2h}) center in MgF₂.^{19,24} The results are shown in Fig. 7. The fit to the experimental data is essentially exact out through the local-mode peak because one-phonon processes are almost totally dominant in this frequency range; the Huang-Rhys factor for the one-phonon processes has the value *S* = 0.3 for the fit shown. Beyond this trivial agreement with experiment in the one-phonon energy range, the fit to the local-mode sideband and the first harmonic of the local mode is reasonably good in view of the extremely simple form assumed for the quadratic coupling coefficients.

The fit to experiment shown in Fig. 7 demonstrates several points. First, a one-phonon peak at $\hbar\omega \sim 0.1$ eV is probably responsible for the corresponding peak in the fluorescence spectrum above the local mode. Second, the convolution of the one-phonon spectrum with itself generates a rather featureless two-phonon band, as shown in Fig. 7(b). The magnitude of the two-phonon spec-

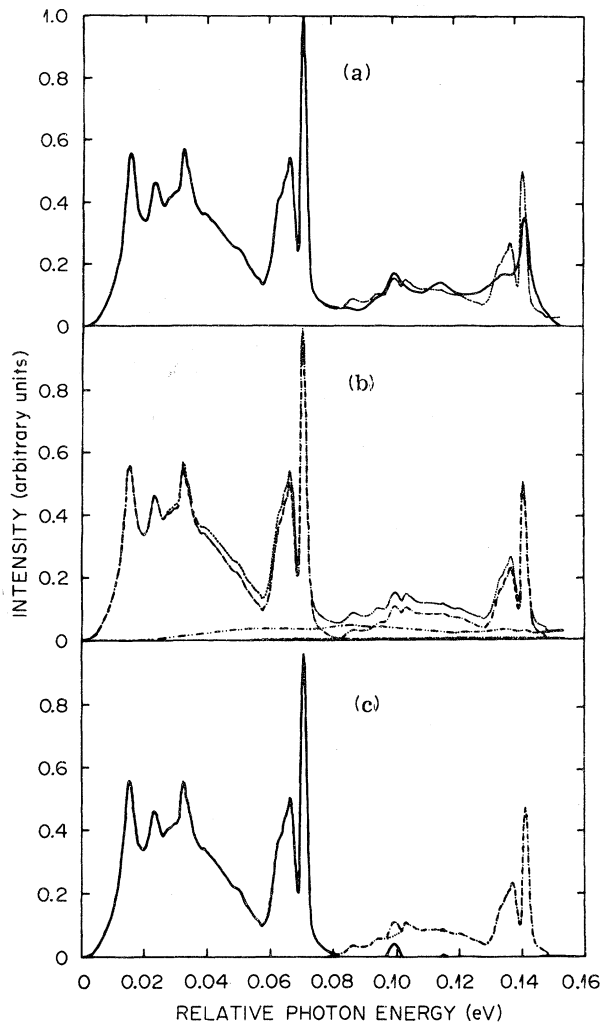


FIG. 7. (a) Fit between the observed (solid line) and calculated (dotted line) vibronic sidebands which was obtained from the simple model described by Eq. (10), with $\alpha = 350 \text{ eV}^{-1}$ and $S = 0.3$. (b) One (dash-dot line), two (dash-double-dot line), and three (dash-triple-dot line), phonon contributions to the calculated total sideband (dotted line). (c) Calculated one-phonon sideband (solid line) and the contribution due to quadratic coupling between the local mode and the lattice modes (dash-dot line).

trum in Fig. 7(b) is small because of the low Huang-Rhys factor for the fit, but a larger Huang-Rhys factor would simply scale up the two-phonon spectrum by a factor of $\frac{1}{2}S^2$ without introducing any further structure in it. In particular, if the Huang-Rhys factor had the value $S = 0.95$ needed to reproduce the observed zero-phonon: total integrated intensity ratio $e^{-S} \cong 0.39$, the two-phonon spectrum would rise to a maximum value of about 0.25 just above the local mode, which is several times larger than the observed spectral intensity

in this region. Third, the local-mode sideband and the local-mode harmonic appear to at least qualitatively replicate many of the features of the one-phonon spectrum out through the local mode.

While the fit to the observed fluorescence spectrum shown in Fig. 7 is reasonably good, it appears to be unrealistic because of the evidence for the importance of forced electric dipole transitions. However, it should be emphasized again that magnetic dipole transitions may make non-negligible contributions to the one-phonon spectrum, and furthermore, that they may dominate in all or part of the two-phonon range. For example, the quadratic coupling explanation just described for the local-mode sideband and the local-mode harmonic may apply even if the entire one-phonon spectrum is produced by forced electric dipole transitions involving odd (T_{1u} and T_{2u}) phonons. The quadratic coupling of the odd local mode with other odd phonons would then yield an even phonon operator which could be involved in allowed magnetic dipole transitions.

The one-phonon vibronic sideband can be used to obtain information on the phonon density of states of the host crystal. However, what is observed directly is an effective density of states, which is the real density of states modified by vibronic selection rules, by the frequency dependence of the electron-phonon coupling parameters, and by the distortions caused by the impurity ions in the lattice. In order to determine the frequency dependence of the electron-phonon coupling parameters, a detailed model must be developed for the lattice dynamics in the presence of the impurity. Such approaches have been carried out for several simple systems,²⁵ but a detailed theoretical treatment of the electron-phonon coupling for the $\text{SrTiO}_3:\text{Cr}^{3+}$ system is beyond the scope of this paper. Instead, we will show only that there is substantial correlation between the observed structure in the one-phonon vibronic sideband and the results of the shell-model calculations of the perfect-crystal density of states.

In the long-wavelength limit, the relation between the effective density of states $g(\omega)$ for vibronic transitions and the phonon density of states $\rho(\omega)$ in the host lattice is $\rho(\omega) = \omega g(\omega)$.^{18,19} Figure 8 shows a comparison between $\omega g(\omega)$ obtained from the one-phonon spectrum in Fig. 7, omitting the local-mode peak, and the perfect-crystal density of states calculated by Stirling.³ The peak positions in the two curves are in generally good agreement. The peak at 0.09 eV in the shell-model results arises from the highest-frequency optic modes. As Stirling notes, the calculated frequencies for these modes are very model dependent, and the particular shell model used for the curve in Fig. 8 (Stirling's model 5) yields a

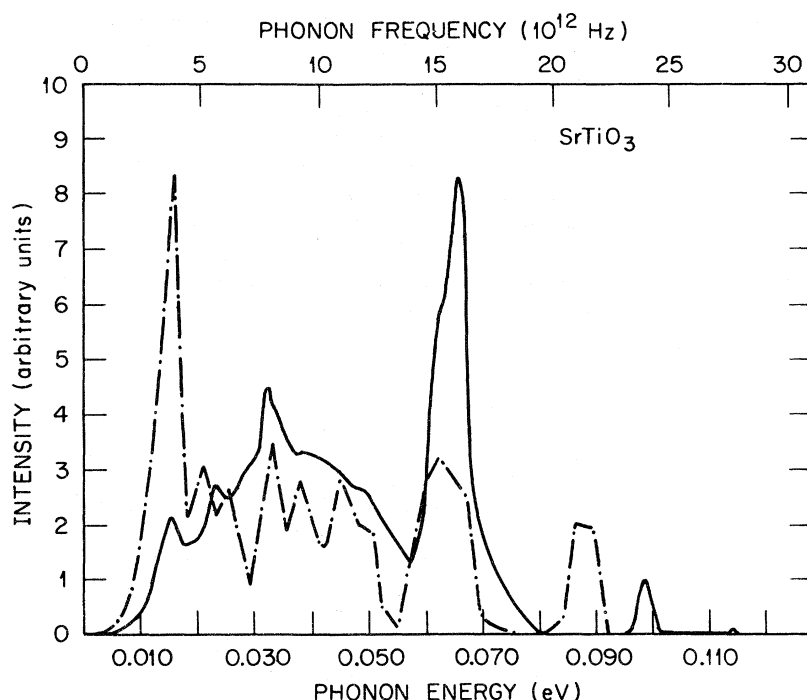


FIG. 8. Phonon density of states of SrTiO_3 calculated from a shell-model fit to neutron scattering data (Ref. 3) (dash-dot line) and obtained from the Cr^{3+} vibronic spectra (solid line).

value for the highest $q=0$ optic-mode frequency which is roughly 10% low (see Fig. 6); the peak should fall at about 0.1 eV as it does in the vibronic density of states. The perfect-crystal peak at 0.0154 eV arises from contributions from phonons around several points in the Brillouin zone. Some of these are forbidden by the selection rules for electric dipole transitions, which may account for the relatively low intensity of this peak in the vibronic density of states.

IV. TEMPERATURE DEPENDENCE OF WIDTHS OF ZERO-PHONON LINES AND LOCAL MODE

The linewidths $\Gamma(R_1)$, $\Gamma(R_2)$ of the zero-phonon lines can be attributed to contributions from several different processes,

$$\begin{aligned} \Gamma(R_i) = & \Delta E_0 + \alpha(R_i) \int d\omega [\omega \rho'(\omega)]^2 n(\omega) \\ & \times [n(\omega) + 1] + \beta(R_i) [\omega_{12} \rho'(\omega_{12})] \\ & \times \{n(\omega_{12}) \delta_{i,1} + [n(\omega_{12}) + 1] \delta_{i,2}\}. \end{aligned} \quad (11)$$

The first term, ΔE_0 , is temperature independent and is due to varying microscopic strains in the crystal. The second term arises from quadratic coupling,^{16,18,19,26} and represents the continual emission and absorption of virtual phonons (i. e., the Raman scattering of phonons) by the impurity ion. In the integrand of this term, $\rho'(\omega)$ is an effective density of states for these processes,

and $n(\omega) = 1/(e^{h\omega/KT} - 1)$ is the thermal occupation number for a phonon of frequency ω . The last two terms are lifetime broadening contributions due to direct electronic transitions between the slightly split components of the initial electronic multiplet in which a real phonon is absorbed or emitted; ω_{12} is the (temperature-dependent) $R_1 - R_2$ difference frequency. The coupling parameters $\alpha(R_i)$ and $\beta(R_i)$ are treated as disposable parameters.

We have attempted to fit our data using three different models for the effective density of states $\rho'(\omega)$ in Eq. (11): a Debye distribution, the vibronic density of states $\omega g(\omega)$ shown as the solid curve in Fig. 8, and an Einstein distribution. The latter represents coupling to only one phonon mode, for this case one of the soft-phonon modes. This model was included because Lüders and Rank²⁷ found that the temperature dependence of the zero-phonon linewidth for europium doped strontium titanate could be explained by coupling only to the soft mode.

Figure 9 shows the measured and various calculated results for the widths of the R_1 and R_2 lines; the plots for the R_2 line are shifted up by one decade in the figure. The experimental values from 80 to 200 K, which is well above the phase transition at 110 K, were obtained by assuming that the R_1 and R_2 lines have the same widths and intensities at these temperatures. The dotted line represents the best fit to the data which could be obtained by using an Einstein mod-

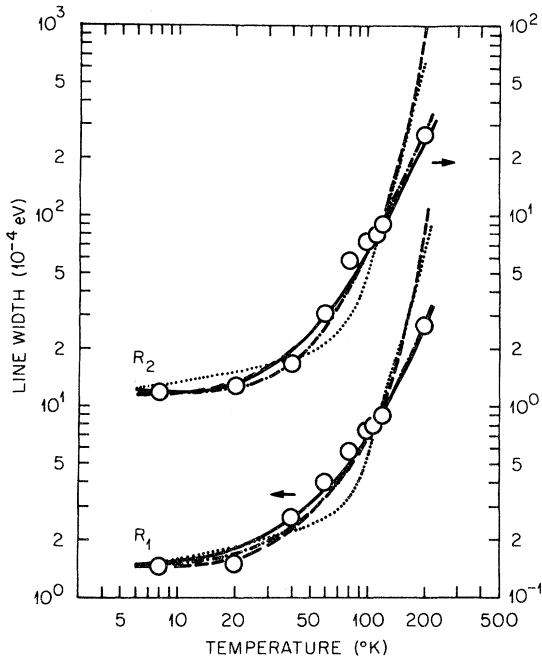


FIG. 9. Temperature dependence of the widths of the zero-phonon lines. Circles represent experimental points. The lines represent the best fits predicted using phonon frequency distributions obtained from the Debye approximation (solid line), the Einstein approximation using the zone-center soft phonon-mode frequency (dotted line), the total one-phonon vibronic sideband (dashed line), and only the first peak in the one-phonon vibronic sideband (dash-dot line).

el for coupling only to the R -point phonon soft mode. Neither this nor coupling to the Γ -point soft mode could be made to fit the data. The dashed line shows the best fit obtained with the vibronic effective density of states $\omega g(\omega)$; this is in reasonably good agreement with the data at low temperatures, but rises too rapidly above the phase transition temperature. The predictions using a Debye distribution are shown by solid lines in Fig. 9. The Debye temperature for the fit is $\Theta_D = 115$ K, which is much lower than the value of 400 K determined from specific-heat measurements. The Debye-model fit is good at all temperatures at which measurements were made. Finally, the dashed and dotted lines were obtained by using the vibronic effective density of states $\omega g(\omega)$, but with an arbitrary upper cutoff imposed at 0.025 eV. This also gives a good fit to the data. These results seem to indicate that low-frequency phonon modes make more important contributions to the zero-phonon line broadening than do high-frequency phonons.

The temperature dependences of impurity-induced local modes are generally investigated

through the use of infrared absorption, but similar studies can be made through the use of vibronic spectra. The width of a local-mode line is affected by microscopic strain and the Raman scattering of phonons as described by the first two terms in Eq. (11). However, some lifetime broadening terms are different for the local mode than for zero-phonon lines. Through anharmonic interactions, the local mode can decompose into two (or more) lattice phonons. This process can be described by^{28,29}

$$\Delta\Gamma_L = \beta_L \int d\omega_1 d\omega_2 [\omega_1 \rho''(\omega_1)] [\omega_2 \rho''(\omega_2)] \times [1 + n(\omega_1) + n(\omega_2)] \delta(\omega_1 + \omega_2 - \omega_L), \quad (12)$$

where $\rho''(\omega)$ is an effective density of states, ω_L is the local-mode frequency, and β_L is a coupling parameter. For fitting purposes, we have further simplified Eq. (12) by assuming that only two modes, with frequencies of 2.6 and 14.8 THz, can contribute; these are the frequencies of the $\text{TO}_1(\Gamma_{15})$ and $\text{LO}_3(\Gamma_{15})$ modes in pure SrTiO_3 , which satisfy the energy-conservation condition in Eq. (12), and which have zero net momentum.

Figure 10 shows the width of the local mode as a function of temperature after the width of the R_1 line has been subtracted out. The dashed line is the contribution due to the decomposition mechanism of Eq. (12), with the additional simplifying assumption noted. Over the temperature range of interest, this contribution is essentially constant. The solid line is the best fit obtained by adding the contributions of the decomposition mechanism and

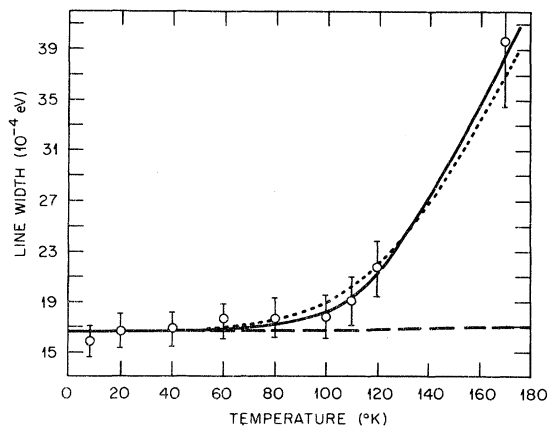


FIG. 10. Temperature dependence of the width of the local mode. The circles are experimental values. The dashed line shows the contribution due to decomposition processes described by Eq. (12), and the solid and dotted lines are the results for the total linewidth obtained using a Debye phonon distribution and the frequency distribution obtained from the one-phonon vibronic sideband, respectively.

Raman scattering (quadratic coupling) in the Debye approximation, with a Debye temperature of 800 K. The dotted line is the similar best fit found by using the total effective vibronic density of states $\omega_g(\omega)$ from Fig. 8 in the Raman scattering term. While the good fits shown in Fig. 10 of both models to the data rest on a number of assumptions made more for reasons of convenience than on physical grounds, they do seem to indicate that both low- and high-frequency phonons contribute to the broadening of the local mode for this system.

V. DISCUSSION AND SUMMARY OF RESULTS

The work described here represents a more detailed investigation of the vibronic spectrum of $\text{SrTiO}_3:\text{Cr}^{3+}$ than has been done previously. More neutron scattering and Raman scattering data have been obtained recently which were not available to earlier workers for comparison with vibronic spectra. Through the use of vibronic selection rules, a number of vibronic peaks were tentatively associated with transitions involving specific phonon modes. Some of the unidentified peaks (especially the low-frequency peaks in the high-energy vibronic sideband) might be associated with phonon modes split by the tetragonal distortion. It would be useful if the symmetry properties of the phonons in the low-temperature phase would be determined.

An area where more work is needed is in developing better theoretical models for predicting the vibronic spectra. From such models, more accurate expressions for the phonon density of states could be obtained. However, the good correlation between the peaks in the density of states obtained from the shell-model fit to the neutron scattering data and that obtained from the vibronic spectrum using the long-wavelength phonon approximation implies that the presence of the impurity ions does

not greatly alter the pure lattice-vibration frequencies.

The most interesting result obtained from analyzing the temperature dependence of the widths of the zero-phonon lines and the local mode was that the former was affected mainly by low-frequency phonons whereas the latter involved phonons of all frequencies. Similar analyses were made of the temperature dependence of the positions of the R lines and the local mode. Although phonon processes can be made to fit the data, there is some question as to the meaningfulness of the interpretation since it has been shown previously that the temperature dependence of the tetragonal distortion makes an important contribution to the shifts of the R lines at low temperatures.^{30,31}

The quadratic coupling should also affect the temperature dependence of the intensity of the local mode. The local mode can be considered as a zero-phonon line and the quadratic coupling region as a one-phonon sideband to this line. As the temperature is raised, more of the emission occurs in the sideband and less in the zero-phonon line. The experimentally measured temperature dependence of the intensity of the local mode has been reported elsewhere³² and fit theoretically using an expression involving a Debye distribution of phonons and a Huang-Rhys factor of 2.9. If the quadratic coupling region of the spectrum can actually be considered as a "sideband" of the local mode, then the Huang-Rhys factor should be given by the ratio of the integrated intensity of the quadratic coupling region to that of the local mode. This is found to give $S=2.11$, which is consistent with the value found from fitting the temperature dependence of the local-mode intensity.

ACKNOWLEDGMENT

It is a pleasure to acknowledge the many helpful comments of R. F. Wood on this work and his critical reading of the manuscript.

*Research sponsored in part by the U. S. Energy Research and Development Administration under contract with Union Carbide Corporation.

†Work done in partial fulfillment of the degree of Doctor of Philosophy. Present Address: Physics Dept., University of North Carolina, Chapel Hill, N. C. 27514.

‡On leave from Physics Dept., Oklahoma State University.

¹F. W. Lytle, *J. Appl. Phys.* **35**, 2212 (1964).

²R. A. Cowley, *Phys. Rev. Lett.* **9**, 159 (1962); R. A. Cowley, *Phys. Rev.* **134**, A981 (1964); R. A. Cowley, W. J. L. Buyers, and G. Dolling, *Solid State Commun.* **7**, 181 (1969).

³W. G. Stirling and R. A. Cowley, *J. Phys. (Paris) Suppl.* **33**, C2-135 (1972); W. G. Stirling, *J. Phys. C* **5**, 2711 (1972).

⁴G. Shirane and Y. Yamada, *Phys. Rev.* **177**, 858 (1969); Y. Yamada and G. Shirane, *J. Phys. Soc. Jpn.* **26**,

396 (1969).

⁵J. M. Worlock and P. A. Fleury, *Phys. Rev. Lett.* **19**, 1176 (1967); P. A. Fleury, J. F. Scott, and J. M. Worlock, *ibid.* **21**, 16 (1968); P. A. Fleury and J. M. Worlock, *Phys. Rev.* **174**, 613 (1968); J. F. Scott, P. A. Fleury, and J. M. Worlock, *ibid.* **177**, 1288 (1969).

⁶H. Unoki and T. Sakudo, *J. Phys. Soc. Jpn.* **23**, 546 (1967).

⁷L. Rimai and G. A. deMars, *Phys. Rev.* **127**, 702 (1962); K. A. Müller, *Phys. Rev. Lett.* **2**, 431 (1959).

⁸M. J. Weber and R. F. Schaufele, *Phys. Rev.* **138**, A1544 (1965).

⁹S. E. Stokowski and A. L. Schawlow, *Phys. Rev.* **178**, 457 (1969).

¹⁰L. Grabner, *Phys. Rev.* **177**, 1315 (1969).

¹¹W. J. Burke and R. J. Pressley, *Phys. Rev.* **182**, 395 (1969).

- ¹²L. A. Vredevoe, Phys. Rev. 147, 541 (1966).
- ¹³Dynamic Jahn-Teller coupling occurs when the initial or final electronic state is a member of a multiplet of degenerate or nearly degenerate levels which are mixed by the electron-phonon interaction in such a way that the electron Hamiltonian within the multiplet cannot be diagonalized by a transformation which is independent of the phonon amplitudes (Refs. 14 and 15). In the cumulant expansion formalism of McCumber (Ref. 16), the lowest-order effects of dynamic Jahn-Teller coupling appear as two-phonon contributions to the spectrum, and as corrections to the spectral moments. Although the initial multiplet (2E_g) of the SrTiO₃: Cr³⁺ fluorescence spectrum can be mixed by dynamic Jahn-Teller interactions with E_g phonon modes, we will neglect this effect because of the evidence that the sidebands are predominantly forced electric dipole in nature, which requires coupling to odd or ungerade phonons.
- ¹⁴F. S. Ham, Phys. Rev. 138, A1727 (1965).
- ¹⁵M. C. M. O'Brien, Phys. Rev. 187, 407 (1969).
- ¹⁶D. E. McCumber, J. Math. Phys. 5, 221 (1964); 5, 508 (1964).
- ¹⁷M. A. Krivoglaz, Fiz. Tverd. Tela. 6, 1707 (1964) [Sov. Phys. -Solid State 6, 1340 (1964)].
- ¹⁸A. A. Maradudin, in *Solid State Physics*, edited by F. Seitz and D. Turnbull (Academic, New York, 1966), Vol. 18, p. 273.
- ¹⁹M. Mostoller, B. N. Ganguly and R. F. Wood, Phys. Rev. B 4, 2015 (1971).
- ²⁰W. G. Spitzer, R. C. Miller, D. A. Kleinman, and L. E. Howarth, Phys. Rev. 126, 1710 (1962).
- ²¹A. S. Barker and M. Tinkham, Phys. Rev. 125, 1527 (1962).
- ²²C. H. Perry, B. N. Khanna, and G. Rupprecht, Phys. Rev. 135, A408 (1964).
- ²³A. S. Barker, Phys. Rev. 145, 391 (1966).
- ²⁴M. Mostoller, B. Henderson, W. A. Sibley, and R. F. Wood, Phys. Rev. B 4, 2667 (1971).
- ²⁵See, for example, W. E. Bron, Phys. Rev. 185, 1163 (1969), and references contained therein; and R. F. Wood and B. N. Ganguly, Phys. Rev. B 7, 1591 (1973).
- ²⁶D. B. Fitchen, in *Physics of Color Centers*, edited by W. Beall Fowler (Academic, New York, 1968), p. 293.
- ²⁷M. Lüders and K. F. Renk, Solid State Commun. 7, 575 (1969).
- ²⁸M. A. Ivanov, M. A. Krivoglaz, D. N. Mirlin, and I. I. Reshina, Fiz. Tverd. Tela 8, 192 (1966) [Sov. Phys. -Solid State 8, 150 (1966)].
- ²⁹R. J. Elliott, W. Hayes, G. D. Jones, H. F. MacDonald, and C. T. Sennett, Proc. Roy. Soc. Lond. A 289, 1 (1965).
- ³⁰J. Slonczewski, Phys. Rev. B 2, 4646 (1970).
- ³¹S. E. Stokowski and A. L. Schawlow, Phys. Rev. 178, 464 (1969).
- ³²Q. Kim, R. C. Powell and T. M. Wilson, J. Phys. Chem. Solids 36, 61 (1975).